Role of surface morphology on bed material activation during indirect gasification of wood

(article starts on next page)

Full Length Article

Role of surface morphology on bed material activation during indirect gasification of wood

Robin Faust [a,*], Ali Valizadeh [b], Ren Qiu [c], Alyona Tormachen [a], Jelena Maric [d],
Teresa Berdugo Vilches [d], Nils Skoglund [e], Martin Seemann [d], Mats Halvarsson [c],
Marcus Öhman [b], Pavleta Knutsson [a]

[a] Department of Chemistry and Chemical Engineering, Chalmers University of Technology, Kemigården 4, 412 96 Gothenburg, Sweden
[b] Energy Engineering, Division of Energy Science, Luleå University of Technology, Luleå SE-971 87, Sweden
[c] Chalmers University of Technology, Department of Physics, Kemigården 1, Gothenburg SE-41296, Sweden
[d] Division of Energy Technology, Department of Space, Earth, and Environment (SEE), Chalmers University of Technology, Gothenburg 41296, Sweden
[e] Thermochemical Energy Conversion Laboratory, Department of Applied Physics and Electronics, Umeå University, SE-901 87 Umeå, Sweden

ARTICLE INFO

ABSTRACT

Olivine and alkali-feldspar were utilized in separate campaigns in an indirect dual fluidized bed gasification campaign with woody biomass as fuel. After three days, both bed materials were reported to be active towards tar removal and exhibited oxygen-carrying abilities and had formed an ash layer consisting of an outer ash deposition layer and an inner interaction layer.

X-ray microtomography analysis concluded that a preferred deposition of ash happens onto convex regions of the bed particles, which results in an increase in thickness of the ash layer over convex regions. This effect is most pronounced for the outer layer which is a product of ash deposition. The inner layer exhibits a homogeneous thickness and is probably formed by interaction of Ca from the outer layer with the particles. Transmission electron microscopy revealed the presence of Fe and Mn on the surface of the particles in a solid solution with Mg. The oxygen-carrying effect which is found for aged particles is therefore attributed to the presence of Fe and Mn on the surface of aged particles. Alkali were found on the surface of both particles which are likely contributing to the catalytic activity of the material towards tar removal.

1. Introduction

Thermal conversion of biogenic fuels can play a major role in reducing fossil CO_2-emissions and the dependence on fossil fuels. Emissions from thermal conversion of biomass can be considered CO_2-neutral, as the CO_2 is reabsorbed from the atmosphere into the biomass during the growth. Biomass is a complex feedstock and a suitable technique for its thermal conversion is based on the utilization of a fluidized bed reactor. Fluidized bed reactors have been assessed to be advantageous compared to other methods in thermal conversion of biomass as they offer higher fuel flexibility [1]. The technology is based on the utilization of fine sand-like particles which are fluidized by a gas stream. This provides a more uniform heat distribution throughout the reactor and improved conversion efficiency.

In fluidized bed gasification of biomass, the oxygen supply to the fuel during the thermal conversion is limited to the level sufficient to cover the heat demand of the conversion by combustion of a part of the feedstock. This results in a product gas containing H_2 and CO which can be applied for further chemical processes. To avoid dilution with combustion products, the energy required for the endothermic gasification reaction can be provided in a dual fluidized bed (DFB) gasification reactor system. DFB gasification is a process consisting of two interconnected reactors which share the bed material while keeping the gases separated. In one reactor, fluidized bed combustion of biomass is conducted where an oxygen-containing gas (e.g., air) is employed as the fluidizing gas. Hence, the bed material will be heated by the exothermic combustion reaction and conveyed by the gas stream into the second reactor where steam or CO_2 is used for fluidization. In this reactor, the hot bed material supplies thermal energy which is required for the endothermic gasification reaction which converts the biomass into the product gas.

One major challenge in biomass gasification is the presence of

polyaromatic hydrocarbons (tar) as side products of the gasification reaction which can cause problems by clogging of the down-stream equipment. Earlier attempts to reduce the concentration of the produced tar in the effluent gas, utilizing a bed material which exhibits catalytic properties has been proven successful [2]. Fluidized beds are most commonly operated with quartz sand (SiO_2); however, quartz does not show catalytic impact towards tar reduction. This is why alternative bed materials, such as dolomite [$CaMg(CO_3)_2$] [2–4], olivine [(Mg, Fe)$_2SiO_4$] [5–7] and feldspar [(K, Na)$AlSi_3O_8$] [8–10] have been examined in fluidized bed gasification. Of those, dolomite has the highest impact in tar reduction. However, as it is comparably softer, the attrition rate will be higher, accordingly [3–4]. On the other hand, feldspar and olivine have shown beneficial behavior towards tar removal without causing problems associated with attrition [7–8].

In addition to the inherent properties of the minerals used as bed material, interactions between the bed material and the fuel ash influence their catalytic properties as well [11]. The ash forms a layer on the bed particles which decreases the concentration of tar in the produced gas. This effect has been extensively reported in the literature and was the focus of a recent review by Kuba et al. [12] For the case of woody biomass, the layer contains elements commonly found in woody biomass ash, which are mostly Ca, K, and Mg. Besides the impact of ash elements added through the fuel, olivine has shown an increase in activity due to different additives, such as salts of potassium [6,13] or calcium [14–15].

In general, when woody biomass is utilized as the fuel, layer formation proceeds by deposition of ash compounds which interact with the bed particles. For the case of quartz, the interaction between ash and bed particles could lead to the formation of alkali-silicates which have a low-melting point and therefore cause agglomeration of the particles [16]. On the other hand, olivine and feldspar are more resistant to agglomeration. For these materials, the interaction of deposited ash particles results in the formation of an interaction layer underneath the deposited ash, commonly denoted as an inner layer. The inner layer has a homogeneous appearance with a composition resembling both bed material and fuel ash. On the surface of the particles, the outer layer is heterogeneous consisting mainly of elements found in the fuel ash. However, ash layer characteristics are dependent on the bed material, fuel ash and the selected conversion process [17–18]. For feldspar, the developed inner layer comprises both Ca-Al-silicates and Ca-silicate while in the outer layer $Ca_3Mg(SiO_4)_2$ and $MgSiO_3$ could be detected [19–20]. In the inner layer formed around olivine bed particles, the formation of $CaMgSiO_4$ was found [17,21]. In both cases, incorporation of higher amounts of Ca into the inner layer structure was associated with cracks in the inner layer perpendicular to the bed particle surface [17,19].

Apart from the catalytic activity, studies investigating the properties of used bed material have shown the development of oxygen-carrying abilities [7,22]. For instance, in DFB gasification, the particles transport oxygen from the combustion side to the gasification side. Although this will decrease the overall calorific value of the product gas, as H_2 and CO could be oxidized to H_2O and CO_2, respectively, the development of oxygen-carrying ability in DFB gasification has been observed to be connected to tar reduction in the product gas [7]. However, it has been shown in a recent study by Pissot et al. [22], that the two effects (oxygen carrying and catalytic activity) are independent, as the utilization of oxygen-carrying bed material (e.g., ilmenite), did not result in lower of the tar yield compared to used feldspar, despite ilmenite's higher oxygen-carrying ability. Regardless of whether the tar decrease is due to catalytic or oxygen-carrying activity or a combination thereof, in either case, surface accumulated species have been considered to influence the properties of the bed material. Thus, it is essential for practical purposes to examine the outermost surface of the particles in more details in order to comprehend the properties of the bed material and how they could be affected by prolonged exposure times.

Most of the aforementioned studies that investigated the activity of the bed materials as a results of layer formation, have focused on the chemical interactions between fuel ash and bed material. Nevertheless, physical properties of the bed particles (e.g., surface morphology) influence the ash layer formation mechanism and consequently alter performance of the bed material in the process. For instance, crack layers in quartz bed particles have been aligned with irregularities over the bed particle surface [23]. Furthermore, the surface morphology has been shown to have a significant impact on surface adsorption processes. Zhu et al. [24] compared two different quartz beds in a floatation separation process. The authors observed that bed material with higher surface area has considerably larger capacity to adsorb sodium oleate due to higher wettability as well as $Ca2^+$ and due to a larger number of adsorption sites. Similarly, the importance of surface morphology of solid particles was demonstrated, for example on the adsorption capacity of different silicates [25–26] or on the wettability of calcite particles [27]. Other studies with similar results have also portrayed the importance of surface roughness on the adsorption behavior of different solid surfaces [28–29]. Even though the cited studies have pointed on the influence of the surface morphology on the material behavior, there is still lack of understanding of how surface irregularities influence the interaction of the bed material with the formed fuel ash and further the development of surface activation (catalytic and/or oxygen carrying). Thus, the current study aims to contribute to filling this knowledge gap.

The commonly employed characterization method for assessment of the surface layer is scanning electron microscopy (SEM). With SEM, it is possible to acquire information about composition and thickness of the layer of several particles, and conclusions about the bed inventory can be drawn by analyzing representative particles. In an earlier study, the formation of an outer layer was found for the used particles, which was only observable with SEM, when cross-sections of the particles were prepared with a more sophisticated sample preparation method, i.e., broad ion-beam milling (BIB) [18]. This study concluded that the composition of the ash layer varies, where a Ca-rich inner layer and a Mg-rich outer layer was found for the utilized bed materials. The outer layer had a thickness of 1–2 μm, which is close to the resolution limit of SEM which is why the resolution of SEM is therefore insufficient for detailed analysis of the outer layer. As the outer layer is in contact with the gas in the gasifier it is decisive for both catalytic tar conversion by the aged bed material as well as the oxygen-carrying ability the material exhibits after prolonged exposures. Another characterization technique which is mostly employed to analyze the particle layers is X-ray diffraction (XRD) which supplements the data from SEM with information on the formation and rearrangement of crystallographic structures of the consisting phases. While XRD is useful to derive general information of the sample, this technique is not surface sensitive and therefore limited in its applicability to draw conclusions about the species which are in contact with the gas phase.

In this study, the discussed shortcomings of SEM and XRD are resolved by the application of transmission electron microscopy (TEM). TEM is utilized to acquire higher resolution images along with the elemental and phase distribution information from the outermost layer around olivine and feldspar bed particles. This is decisive to list out which elements are in contact with the gas phase in the reactors and therefore participate in the previously listed characteristics of aged bed material, i.e., catalytic activity and oxygen-carrying ability. Additionally, TEM diffraction offers the possibility to obtain surface sensitive crystallographic information. Furthermore, X-ray microtomography (XMT) was employed to investigate the effect of surface morphology on the bed particle layer formation and to obtain a 3D understanding on how the layer is distributed over the bed particle surface. Apart from novel knowledge, the present study demonstrates the importance to use the different methods complementary to each other and derive conclusions from similarities that are observed.

Table 1

Chemical composition of the investigated bed materials given in mol percentage on an oxygen free basis, according to the suppliers.

mol %	Olivine	Feldspar
Na		7.56
Mg	60.48	0.05
Al	0.44	20.10
Si	34.11	61.25
P		0.06
K		9.72
Ca		1.17
Ti		0.01
Cr	0.20	
Fe	4.55	0.08
Ni	0.21	

2. Materials and methods

2.1. Experimental campaigns

This study investigates olivine and feldspar which were utilized as bed materials. Their elemental composition is shown in Table 1 and the particles size distribution in Fig. 2. The fresh bed material is mined as rocks and crushed to the desired particle size. Olivine is a solid solution of Mg_2SiO_4 (forsterite) and Fe_2SiO_4 (fayalite), corresponding to $Mg_{1.86}Fe_{0.14}SiO_4$. The feldspar used for this study is an alkali-feldspar and consists of 48 % K-feldspar ($KAlSi_3O_8$), 40 % Na-feldspar ($NaAlSi_3O_8$), 6 % Ca-feldspar ($CaAl_2Si_2O_8$), and 6 % quartz (SiO_2). Each bed material was utilized in a separate experimental campaign conducted in the Chalmers dual fluidized bed gasifier (see Fig. 1), which consists of a 2–4 MW$_{th}$ bubbling fluidized bed gasifier (6) and a 12 MW$_{th}$ circulating fluidized bed combustor (1). The temperature ranges between 800 and 850 °C. Woody biomass was utilized as fuel; 2 t/h of wood chips were fed to the combustor and 300 kg/h of wood pellets were fed to the gasifier.
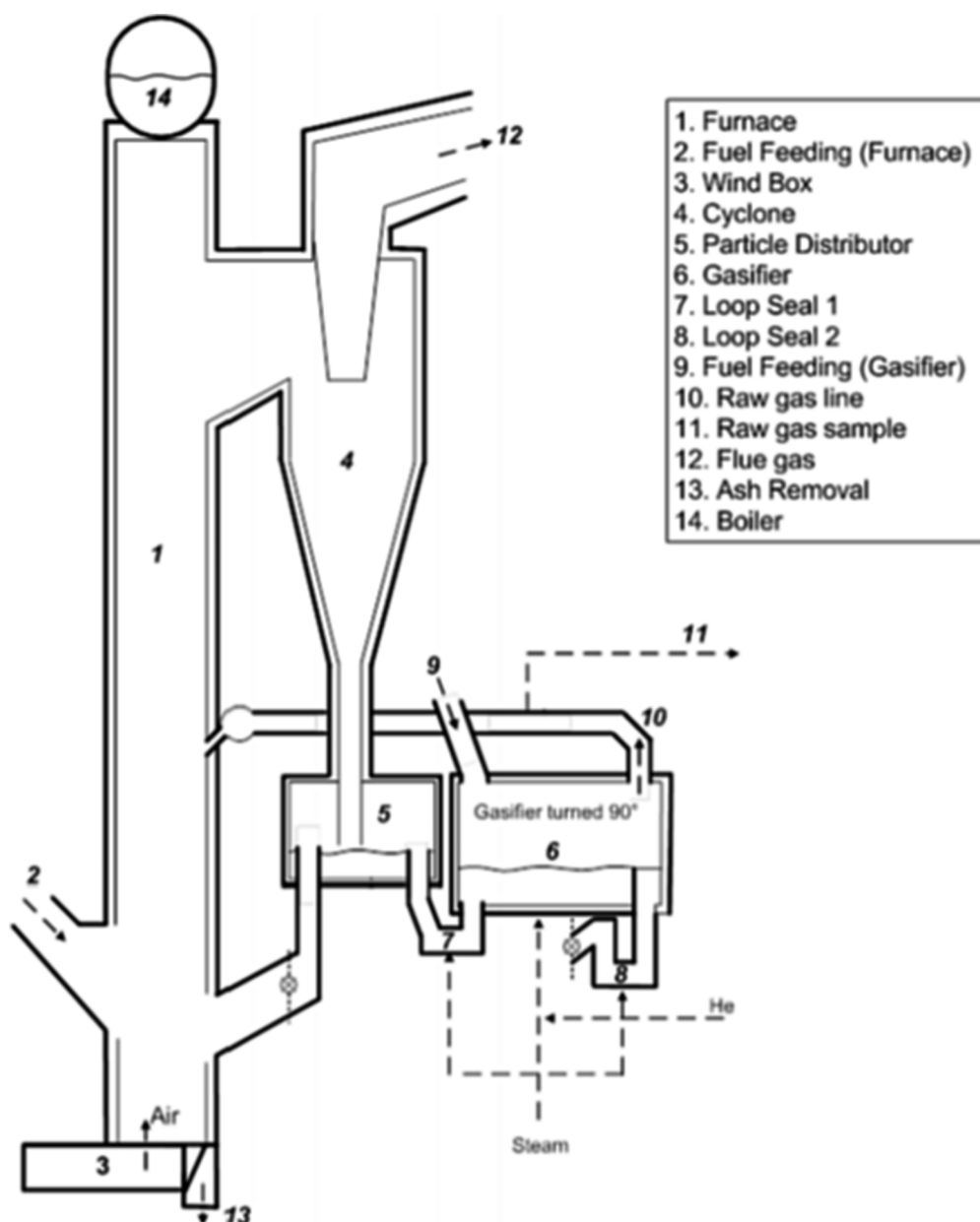

1. Furnace
2. Fuel Feeding (Furnace)
3. Wind Box
4. Cyclone
5. Particle Distributor
6. Gasifier
7. Loop Seal 1
8. Loop Seal 2
9. Fuel Feeding (Gasifier)
10. Raw gas line
11. Raw gas sample
12. Flue gas
13. Ash Removal
14. Boiler

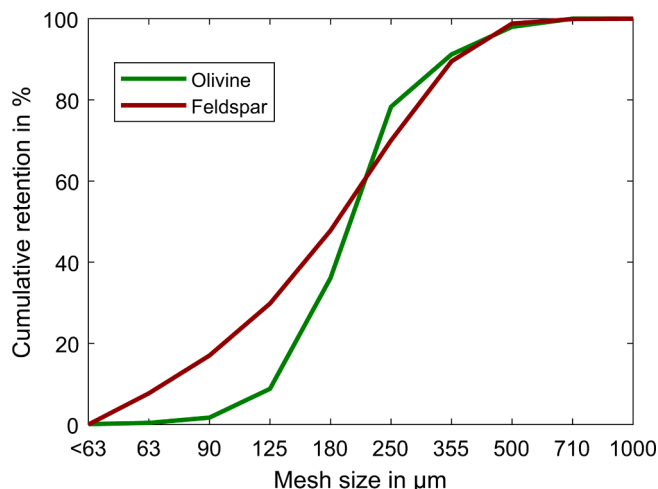**Fig. 1.** Schematic representation of the Chalmers DFB gasifier [1].

Fig. 2. Particle size distribution of the fresh materials according to the suppliers.

Table 2

Ash composition of the feedstock (dry fuel basis) used during the experimental campaigns from which the bed material samples were extracted. The wood chips (0.5 wt% ash) were fed to the furnace, the wood pellets (0.4 wt% ash) were fed to the gasifier.

	Wood Chips [mmol/kg]	Wood Pellets [mmol/kg]
Na	1.3	2.2
Mg	7.0	9.1
Al	1.5	0.7
Si	5.7	2.8
P	2.3	3.2
K	10.2	21.0
Ca	25.0	32.4
Ti	<0.2	<0.2
Mn	2.2	1.1
Fe	0.7	0.4
Ba	0.1	0.1

The ash composition of the fuel is shown in Table 2. The bed samples were extracted after 3 days residence time from the loop seal located after the gasifier (7). No addition of fresh bed material was performed during the experimental campaign in order to ensure the specified age of the bed particles. Note that in the case of the experiment with olivine, a solution of ammonium sulfate was added to the cyclone to control the emissions of CO. A summary of the exposure conditions is given in Table 3.

In the Chalmers semi-industrial DFB system, about 4 tons of bed material are circulating. Of the samples taken from the bed inventory, only about 1 – 10 g of sample is usually used for XRD analysis. Using the commonly employed epoxy embedding method for the preparation of a sample investigated with SEM, around 100 – 1000 particles can be analyzed (~1 – 10 mg); even fewer particles (around 10) can be prepared and analyzed when the previously mentioned BIB method is employed. The number of particles analyzed with XMT is comparable with SEM, where XMT offers the advantage of 3D imaging. TEM offers the possibility of higher resolution, however, with the trade-off that only

a small fraction of the layer on one particle can be analyzed. The different techniques are therefore required complementary to each other. The statistics in analysis as limitation in sample characterization is exemplified in Fig. 3.

2.2. Electron microscopy characterization

To reveal cross-sections of the bed particles, broad-ion beam (BIB) milling was employed where around 10 particles for each bed material were fixated separately between two silicon wafers and subsequently polished with a Leica EM TIC 3X. The particles were subsequently analyzed by scanning electron microscopy (SEM) with the back-scattered electron (BSE) signal. The BSE signal strength depends on the average atomic number of the investigated location, where heavier elements result in a stronger signal (i.e., brighter contrast). A FEI Quanta 200 FEG SEM was used which was equipped with an energy dispersive X-ray spectroscopy (EDS) system. 15 kV acceleration voltage was applied for imaging and EDS analysis and the low vacuum mode was utilized with 20 Pa water as charge neutralizing gas.

More detailed microstructures were studied by (scanning) transmission electron microscopy (STEM/TEM) on the thin foil samples, using an FEI Titan 80–300 TEM/STEM instrument. The thin foil samples were prepared using an FEI Versa3D focused ion beam – scanning electron microscopy (FIB – SEM) instrument equipped with an Omni-probe micromanipulator. In the TEM mode, bright field (BF) imaging and selected area electron diffraction (SAED) were performed with a Gatan US1000 charge-coupled device (CCD) camera. STEM imaging was performed with a BF detector and a high angle annular dark field (HAADF) detector. EDS data was collected in STEM mode using an Oxford X-sight detector.

2.3. X-ray microtomography Analysis.

X-ray Microtomography (XMT) utilizes X-rays to produce 2D image cross sections of an object, which can be combined to recreate a 3D image of the probed material. Images produced through XMT portray optical density of the scanned object meaning that the image is constructed from relatively darker and brighter areas which resemble lower
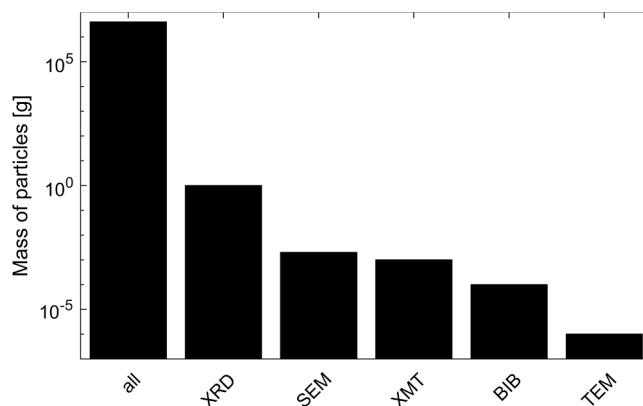

Fig. 3. Estimated fraction of sample (log-scale) usually analyzed with the different characterization techniques.

Table 3

Summary of the exposure conditions of the two materials investigated in this study. The materials were exposed to the same environment except for the addition of ammonium sulfate to control CO emissions in the case of olivine.

Bed Material	Formula	Combustor		Gasifier		Interval	Additives
		Fuel	Rate [t/h]	Fuel	Rate [kg/h]		
Olivine	$Mg_{1.86}Fe_{0.14}SiO_4$	Wood Chips	2	Wood Pellets	300	3 days	Ammonium Sulfate
Feldspar	$(K, Na)AlSi_3O_8$	Wood Chips	2	Wood Pellets	300	3 days	None

Fig. 4. Terms used in this study to describe the different layers.

and higher densities, respectively. Moreover, other physical properties of the sample including surface area, volume and volume fraction of different phases could also be measured. A plastic tube with 1 mm diameter was used as the sample holder. 2 mm of the tube's height was filled with the bed particles and left for 16 h in order to neutralize the sample from any possible electric charges. Feldspar and olivine samples were separately inserted into the XMT machine (Xradia 620 Versa) with the optical resolution of 0.8 µm which provided a field of view covering around 15 bed particles. The scanning was performed with an X-ray tube voltage of 40 kV and 3 W tube power with a LE3 X-ray filter from Edmund industrial optics. During each scan, 2001 projection radiograph images were acquired over 360° sample rotation with 10- and 9-seconds exposure time for olivine and feldspar, respectively.

Raw data from XMT characterization were exported to DragonFly software (version 2020.2 build 941), where X-ray scans from several planes of the sample could be combined to create a 3D image of the entire sampling tube. Contrast difference (Fig. 9 left) and pre-installed color filters (Fig. 9 right) were used to distinguish difference in density phases where each color denotes a certain optical intensity in the studied object. To gauge the bed layer thickness around over the bed particle surface, a pre-installed thickness measurement feature in the software was utilized.

2.4. Batch reactors

The oxygen-carrying ability of the fresh and used bed material was
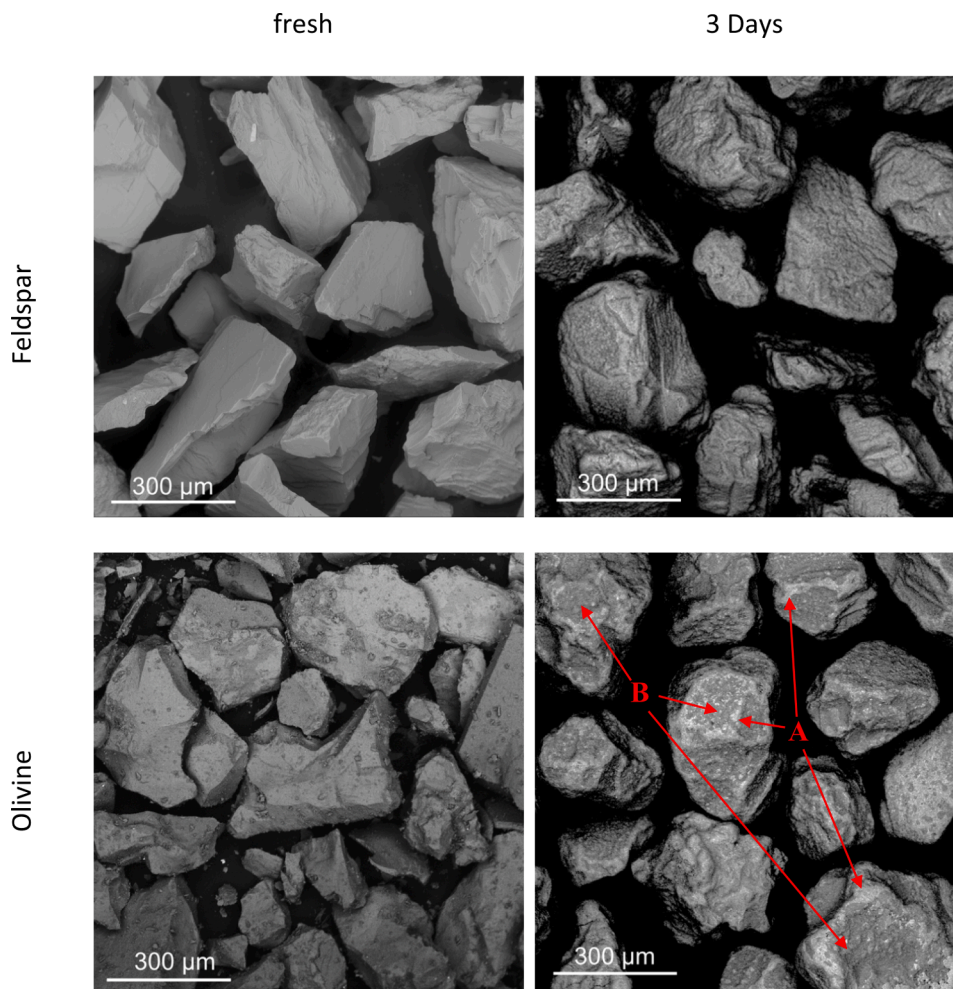

Fig. 5. Back-scattered electron micrographs of the particles before and after exposure. The fresh particles exhibit rugged features and sharp edges, which disappear after 3 days residence time in the gasifier. A and B indicate locations with difference in morphology that have been formed as a result of introduction of additives to the process.
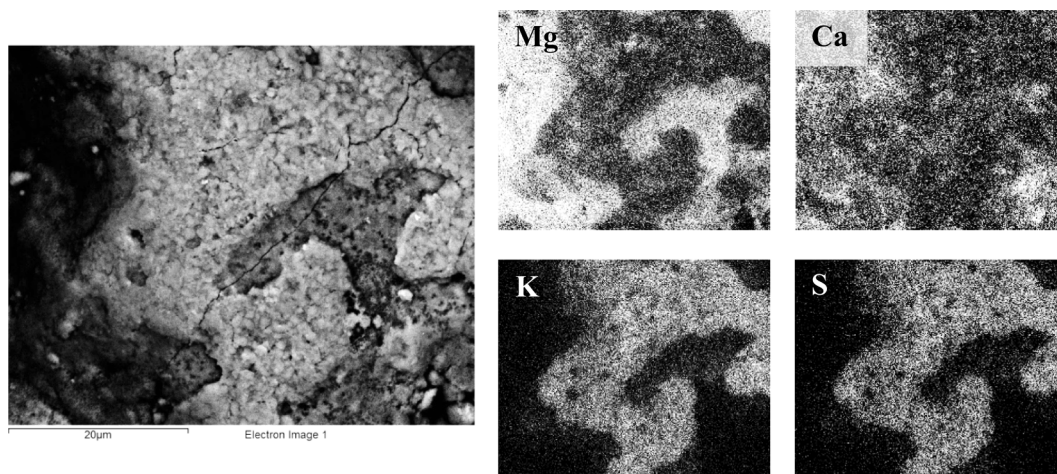
Fig. 6. BSE overview and elemental intensity maps acquired by SEM-EDS on the surface of olivine particles which have remained in the gasifier for 3 days. A phase rich in K and S (probably K_2SO_4) is deposited onto the edges of the particles. This phase has most likely formed to due to the addition of ammonium sulfate in the case of olivine.

investigated in a laboratory-scale batch fluidized bed reactor using 15 g of the bed particles in each experiment. The gas stream applied for fluidization was alternated between oxidizing, inert, and reducing. The reactor was electrically heated and maintained at 850 °C during the test. More details about the laboratory set-up can be found elsewhere [30]. Each bed sample was exposed first to an inert atmosphere (N_2) for 300 s and subsequently oxidized with 5 % O_2 in N_2 for 600 s to fully oxidize

the elements which can contribute to the oxygen-carrying ability of the material. The remaining O_2 was purged with another inert (N_2) in the next step for 300 s after which the reduction step was conducted. The reduction was done with syngas (50 % CO and 50 % H_2) which is representative of the atmosphere during biomass gasification. The difference in O_2 entering and leaving the reactor during the oxidizing step (after the material had been exposed to the reducing atmosphere) was
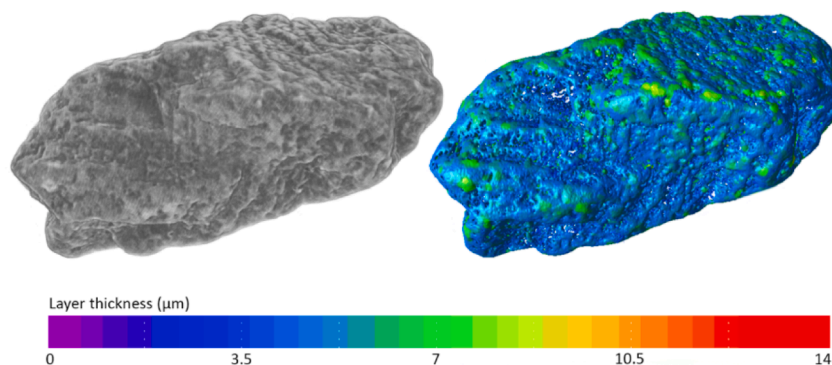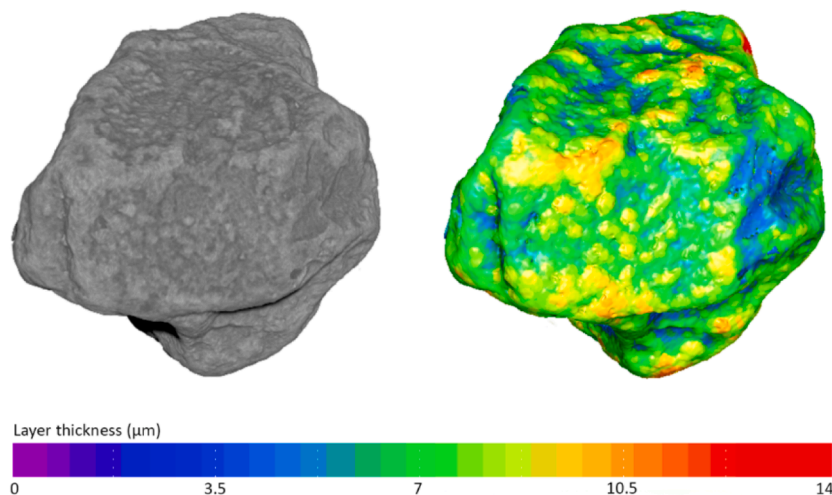

Fig. 7. 3D XMT image of the overall bed layer thickness of a bed particle that after 3 days residence time in the gasifier. The layer thickness measurement is shown (right) and compared to the XMT image from the same bed particle (left) for (a) feldspar and (b) olivine.
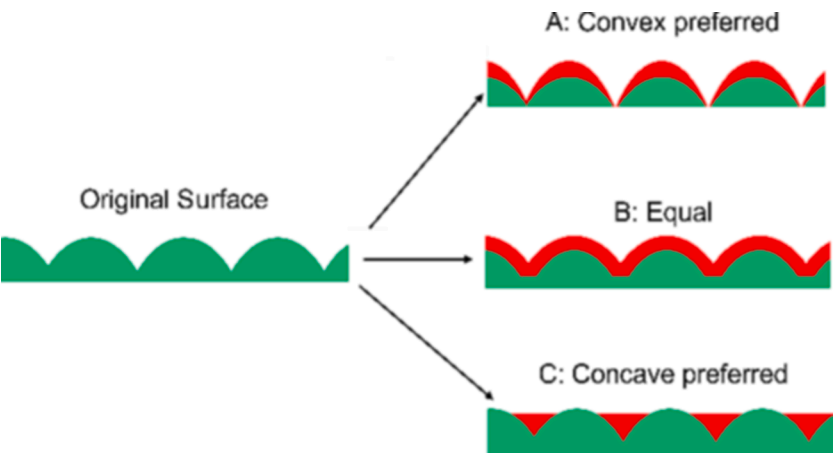
Fig. 8. Schematic representation of the possible layer formation locations.

measured to obtain comparable results on the oxygen-carrying ability of the material.

2.5. Nomenclature

A multitude of studies exist which investigate and describe the layers formed by the interaction of different bed materials with different fuels. To facilitate a comparison between publications from different research groups, the terms used in the current study are defined in Fig. 4.

The term "ash layer" is used here as the sum of all layers around the bed particles formed due to interaction and deposition of ash compounds.

The "outer layer" is used to refer to the layer commonly described as inhomogeneous and formed by ash deposition.

The "inner layer" is used to refer to the layer commonly described as homogeneous and formed by the interaction of the deposited ash and the
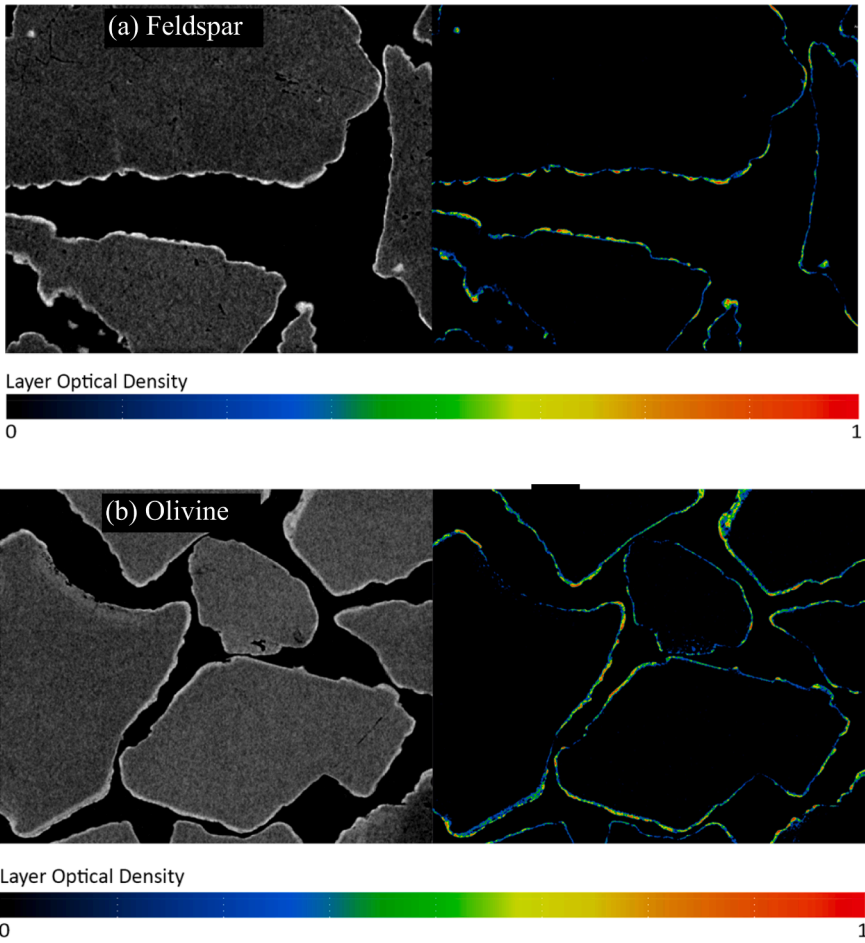

Fig. 9. XMT measured density distribution in the bed particle layer (right) compared to the 2D cross-sectional view of the exact same plane (left) for a typical (a) feldspar and (b) olivine bed particle. The measured relative optical densities were normalized where 0 represents the lowest detected density and 1 represents regions with the relatively highest density in the analyzed sample.

Table 4
Physical properties of the bed materials measured with XMT.

Bed material	total bed sample volume (mm³)	total bed sample surface (mm²)	specific surface (mm²/mm³)
Olivine	0.48	12.40	25.83
Feldspar	0.46	18.74	40.74

bed particle.

The "bulk" describes the bed particle with a composition similar to the fresh bed material.

3. Results and discussion

3.1. Morphology

Both bed materials are mined as rocks and crushed to the desired particles size prior to utilization in the gasifier. Therefore, they exhibit sharp edges in their fresh state (see Fig. 5, left). After three days of exposure time, the particles appear to be much smoother, which was attributed to either attrition [6,15,31] and ash layer formation [8,14,32] or both [19–21] in previous studies. While the aged feldspar exhibits quite uniform BSE contrast, aged olivine exhibits two features of different contrast (indicated with **A** and **B** in Fig. 5). Region **A** is preferentially located on the edges of the particles, whereas **B** is located mostly on the particles' sides. An EDS intensity mapping (shown in Fig. 6) reveals that region **A** contains significantly higher concentrations of K and S compared to region **B**. As this behavior was found only in olivine but not for feldspar, the difference in exposure history (i.e., the addition of ammonium sulfate) could be attributed to the formation of K- and S-rich regions. Therefore, addition of ammonium sulfate can be attributed to cause deposition of a K- and S-rich phase. EDS point

analysis within this location showed a molar ratio of K:S of about 2 which agrees with the formation of K_2SO_4, which was also found with XRD in the previous study of the material [18].

XMT allowed to confirm the smoothening which both samples exhibited, and attribute it to layer formation. Further, XMT analysis allowed to appreciate the layer thickness formed around the individual bed material particles. Fig. 7 shows the layer thickness measurement result for typical feldspar and olivine bed particles, respectively. A color graphed image for the layer thickness is represented side by side to the original bed particle in the figure so the layer thickness over different surface morphologies of the bed particle could be observed. Comparing the two figures reveals that the average layer thickness is higher on olivine than on feldspar. Yet in both cases, there is a noticeable difference in the layer thickness upon the convex and concave areas over the bed particle surface. Based on the differences in the surface morphology, three different possibilities for layer build-up have been identified. The three possibilities of layer formation depending on surface morphology are schematically shown in Fig. 8. From the XMT analysis, it can be seen that the convex shaped regions possess a thicker layer meaning that there is a higher tendency towards layer formation in these areas (represented by mechanism "A" in Fig. 8). This effect can be observed in more detail on the cross-sectional views, shown in Fig. 9. Furthermore, it could also be observed that the frequency of the convex and concave areas is higher in the case of feldspar. This was attributed to the higher surface roughness which leads to less uniformity in the layer thickness around the feldspar bed particles compared to olivine.

The surface roughness was quantified with XMT by measuring the total bed volume and the total bed surface. Thereby the specific surface area for both bed samples through the entire sampling tube was calculated and represented in Table 4. Comparing the specific surface areas of both bed materials reveals that the same volume of feldspar exposes ~50 % more surface area than olivine which means that feldspar
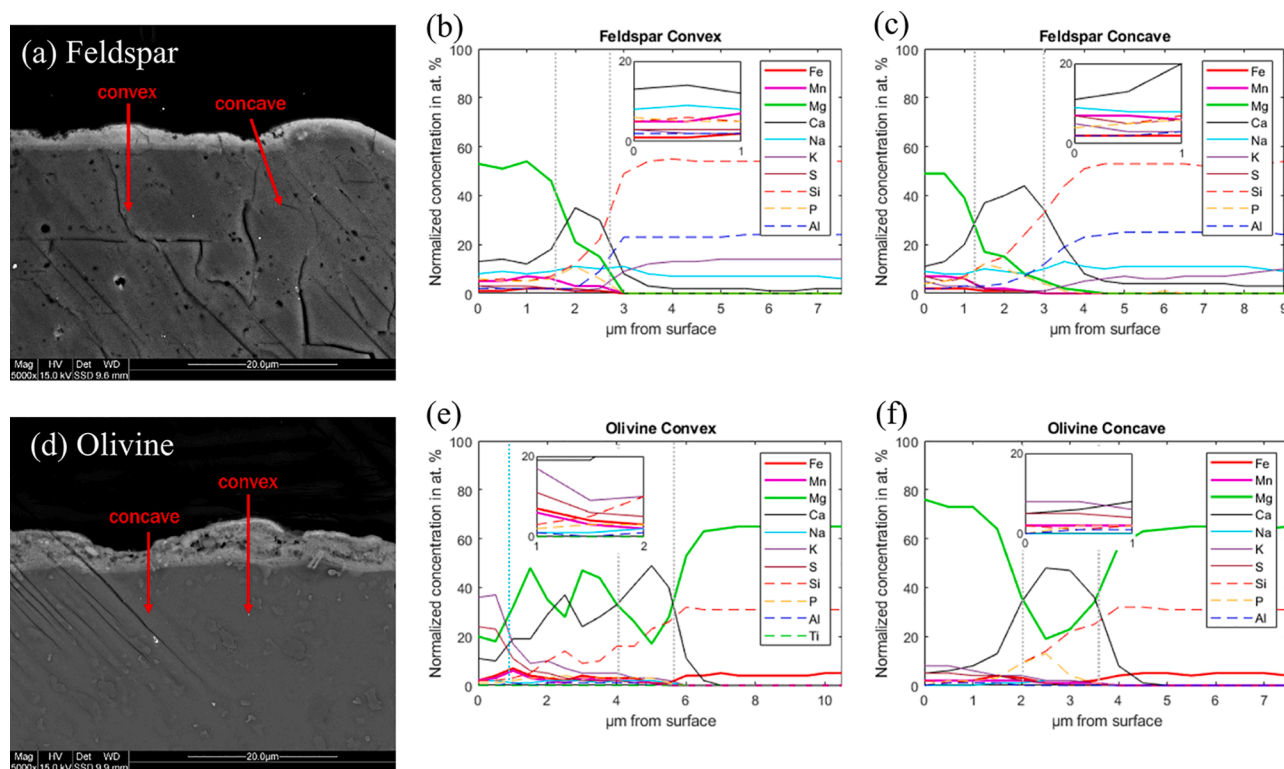

Fig. 10. Back-scattered electron micrographs of typical ash layers formed on feldspar (a) and olivine (d). EDS line-scans (shown in atomic %) were recorded on a convex and a concave location in the ash layer. The normalized elemental compositions are shown in (b) and (c) for feldspar and (e) and (f) for olivine. The two dashed grey lines indicate the location of the "inner" layer. The cyan line in (e) indicates the location of the K- and S-rich layer. The inset shows the concentration of minor elements on the topmost 1 µm; in figure (e) underneath the K- and S-rich layer (i.e., between 1 and 2 µm from the surface). (For interpretation of the references to color in this figure legend, the reader is referred to the web version of this article.)
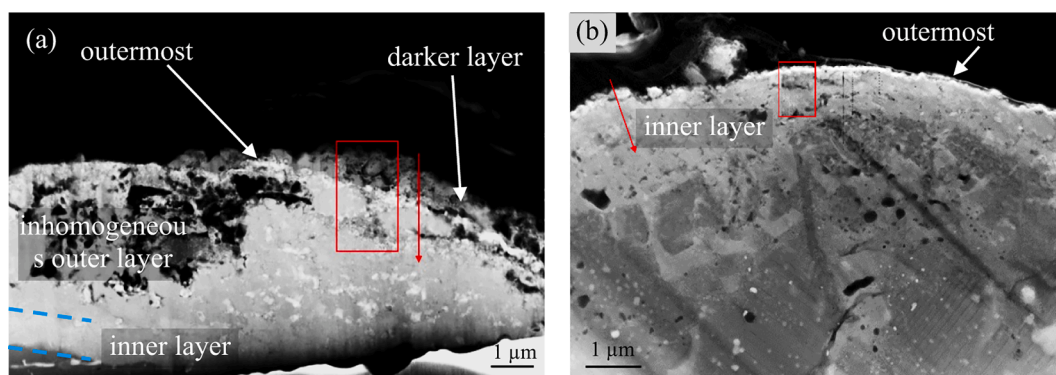
Fig. 11. Overview TEM micrographs of the two samples investigated. (a) olivine, (b) feldspar. The location of the EDS-mapping (as shown in Fig. 12) and the EDS line-scan (as shown in Fig. 13) are indicated in red. (For interpretation of the references to color in this figure legend, the reader is referred to the web version of this article.)

exhibits relatively higher surface roughness. However, the volume fraction of the total layer volume around the bed particles was measured to be 0.078 for olivine and 0.049 for feldspar showing ~50 % thicker bed layer formation for the olivine. This can be decisive for the catalytic activity of the bed material as the surface area of aged bed material can have a stronger impact on their catalytic activity towards the water–gas shift reaction than the concentration of ash elements [9].

3.2. Elemental composition

The analysis with XMT has shown the importance of the morphology of the layer, where thicker ash layers are formed on convex locations. To compare the elemental composition on convex and concave locations, EDS line-scans were recorded on both materials and the results are shown in Fig. 10. Both materials exhibit the typical formation of a homogeneous inner Ca-rich layer which has a constant thickness of around

1–2 μm [12,17–21,32–35]. This layer can be found on both convex and concave locations and is indicated as the location between the two dashed grey lines in the EDS line-scans shown in Fig. 10. The constant thickness and composition suggest that this layer is growing inwards into the original bed particle [34]. However, the materials differ regarding the formation of the outer layer. This layer is usually described as inhomogeneous in thickness and associated with the deposition of ash particles and therefore often resembles the fuel ash composition [23,32–33,36–38]. It can be speculated that the ash-derived Ca migrates from the deposited outer layer into the original bed particle, thereby forming the homogeneous inner layer. For the case of the convex layer on olivine, the previously discussed deposition of a K- and S-rich phase (most likely K_2SO_4) is indicated with the cyan line. The difference in curvature of the layer appears to be related to the thickness of the outer layer: while the inner layer is almost homogeneous in thickness (following mechanism "B" in Fig. 8), the outer layer is
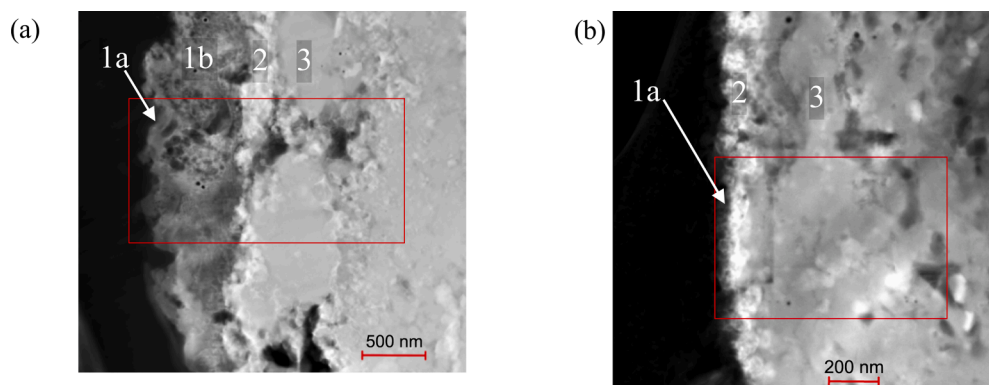

Fig. 12. TEM dark-field micrographs of (a) olivine and (b) feldspar, recorded at the locations indicated with the red box in Fig. 11. An EDS elemental intensity map is shown below which was recorded at the locations indicated inside the red box. The numbers illustrate the similarities in layer composition. layer **1** is rich in alkali or alkaline earth metals; layer **2** contains transition metals (Fe and Mn) and Mg; layer **3** is rich in Si and P. (For interpretation of the references to color in this figure legend, the reader is referred to the web version of this article.)
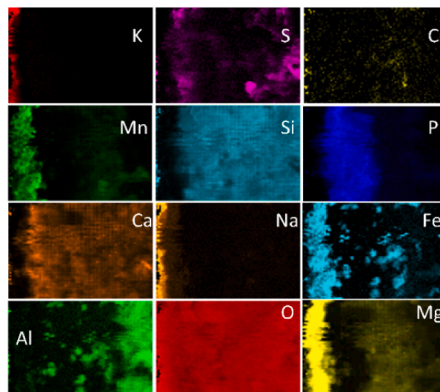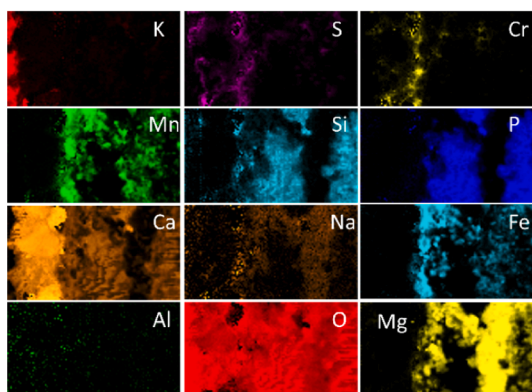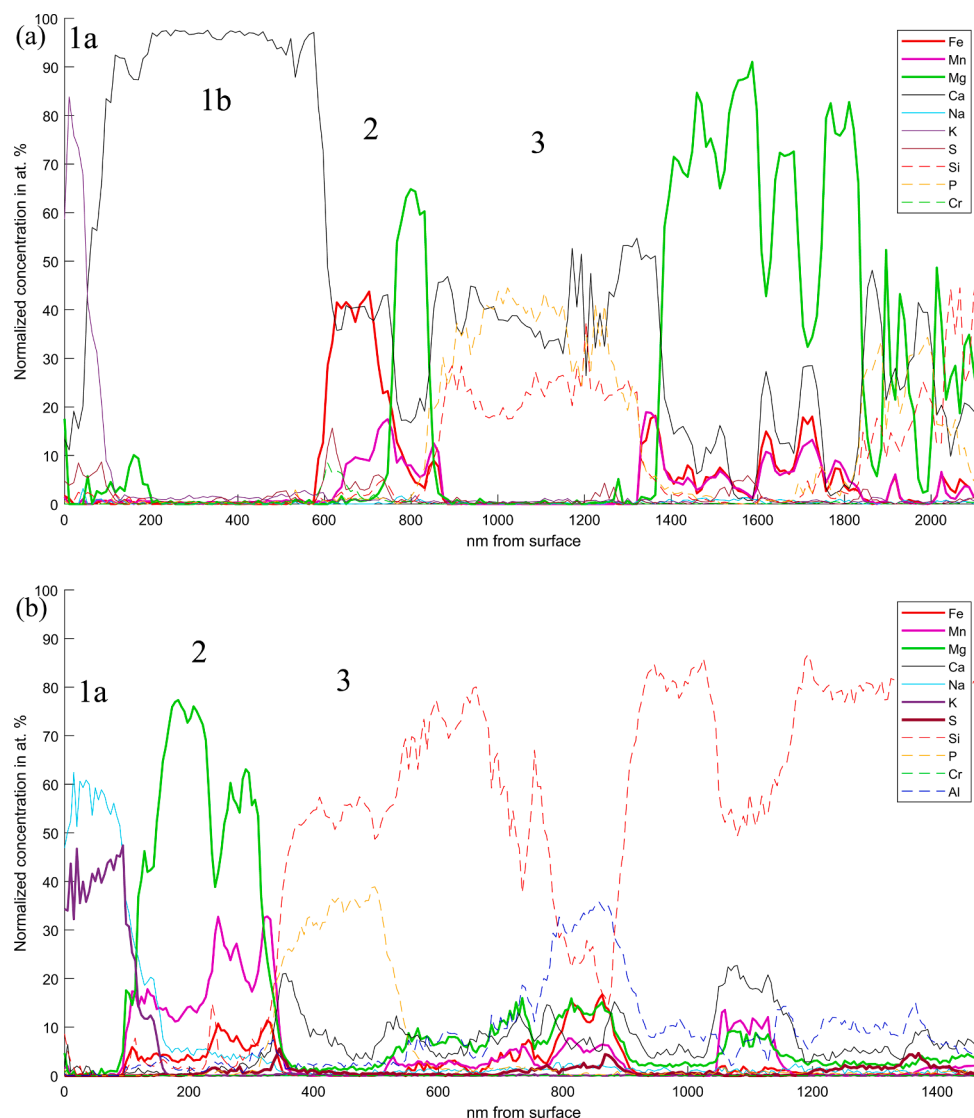
Fig. 13. EDS line-scans at the outermost part of the layer at convex locations indicated as red squares in Fig. 11. (a). olivine, (b). feldspar. The data is normalized and presented on a C- and O-free basis. (For interpretation of the references to color in this figure legend, the reader is referred to the web version of this article.)

thicker on the convex areas (mechanism "A"). The deposition of K_2SO_4 occurred preferentially on the convex location which agrees with the previously discussed stronger tendency of layer formation on convex locations. The morphology is therefore decisive for the formation of the outer layer, which is associated with deposited ash-derived elements.

Generally, around 50–70 at. % Mg can be found in the outer layer as well as 10 at. % Ca and 5 at. % Mn. Al is almost absent in both the fuel ash and the outer layer, which supports the suggested formation of the outer layer by ash deposition. Unlike olivine, around 10 at. % Na can be found on the surface of feldspar which suggests a driving force of diffusion of Na from the bulk feldspar towards the surface. Similarly, a small increase in Fe appears to be present on the surface of convex olivine. Together with the Mn found on both samples, this could contribute to the oxygen-carrying ability of the bed material.

3.3. Surface analysis

To investigate the surface of the particles in more details, a TEM lamella was lifted out from one of the particles. The choice of location for the lift-out was made based on the previous results acquired with SEM and XMT. A convex location was chosen for both samples, to investigate the underlying reason for the amplified layer formation in

more details. For the case of olivine, a location free of the K- and S-rich layer was selected, to investigate similarities between the two materials independent of their exposure history.

Overviews of the olivine and the feldspar samples are shown in Fig. 11 (a) and (b), respectively. As it was presented in our previous study, [18] olivine exhibits an ash layer of around 4 – 7 μm thickness after 3 days of interaction with woody biomass ash. The lift-out was done on the ash layer, where only a small part of the bulk olivine can be observed in the bottom left corner of the micrograph [Fig. 11 (a)]. The homogeneous inner layer of around 1–2 μm thickness can be seen adjacent to the bulk olivine (as indicated with the dashed blue line). Above the inner layer, a heterogeneous outer layer was observed. Again, this agrees with the previously listed studies on the interactions between olivine and woody biomass ash. The higher resolution achieved by the current analysis enables the differentiation of several features within the inhomogeneous outer layer. An outermost layer, brighter in contrast, which was found previously [18] is visible and covers the entire sample. However, contrary to our previous results, another darker layer can be detected on the sample. The feldspar sample exhibits an inner layer with around 2 – 3 μm thickness after 3 days of exposure, which is also similar to our previous study [18]. Again, an outer layer could be observed as a line brighter in contrast. Both samples were further investigated with

Table 5
Phases identified with TEM diffraction on the layers denoted according to Fig. 13.

Sample	Layer	Phase
Olivine	1b	$CaCO_3$
Olivine	2	Mn_2O_3
Feldspar	2	MgO and Fe_2O_3
Feldspar	3	Amorphous

TEM-EDS which is shown in Fig. 12 and Fig. 13.

Fig. 12 (a) and (b) portray EDS elemental intensity maps for olivine and feldspar, respectively. The location selected for olivine was at the previously mentioned darker phase, which is denoted as **1b** in Fig. 12. As can be seen from the intensity maps, this layer mainly contains Ca and O. This was confirmed with the EDS line-scan (Fig. 13), where the results are normalized to a C- and O-free basis. The presence of Ca on the surface is commonly found to improve the catalytic activity of bed materials [8,14–15,39–40]. However, both map and line-scan reveal the presence of yet another layer above this Ca-rich layer which exhibits a high concentration of K. In Fig. 12 (a), this layer is denoted as **1a**. The presence of K on the surface of olivine particles was found previously by Knutsson et al. [6] and the interplay of Ca and K was suggested to be responsible for the observed catalytic activity towards reduction of tars. A similar layer consisting of alkali was found for the case of feldspar, where both K and Na were found to be present. Alkali are known to decrease the tar concentration in the product gas [8,41–43] which is why their presence at the surface of the particles could be a possible explanation of the observed catalytic activity of the investigated particles.

The presence of a layer consisting of Mg, Mn, and Fe can be observed for both materials underneath layers **1a** and **1b**. This layer is denoted as **2** in Fig. 12 and Fig. 13. The migration of Fe to the surface of olivine particles is a known phenomenon in the literature [2,15,44] and the formation of a Mg-rich surface layer has also been discovered previously [18,44]. According to Berguerand et al. [8] where the process parameters of the feldspar used for this study are investigated, the bed material develops an oxygen-carrying ability at later stages of the experiment. As a consequence, the concentration of H_2 in the syngas and the heating value of the product gas will be decreased which is not desirable in the gasification process. The coincidence of Fe together with CaO or MgO was found to have synergistic effects regarding both oxygen-carrying ability of the bed material and its catalytic activity [42,45–46].

3.4. Diffraction

To identify the crystallographic phases which are present at the surfaces of the particles, an attempt was made to record and assign the electron diffraction patterns obtained with TEM. Due to the complexity of the elemental composition of the surface layer, this is a challenging endeavor. The layers indicated with **1a** were too thin for both samples to record any diffraction patterns. The phases that were identified in the respective layers are shown in Table 5. This list is not exhaustive and should be treated as a result of some of the phases which have formed on the surface. The diffraction patterns and the matched phases can be found in the supplementary material.

$CaCO_3$ was found on the surface of olivine which agrees with the elemental composition shown in Fig. 13, where the data is presented on a C- and O-free basis. The presence of $CaCO_3$ can be beneficial for the catalytic activity of the material and was found by Kuba et al. [44] with Raman spectroscopy during surface analysis of ash-layered olivine. On the oxygen-carrying layer (denoted **2**), Mn_2O_3 was a possible match with the recorded pattern. Mn_2O_3 can form a solid solution with Fe_2O_3 and is therefore a possible phase corresponding to the elemental composition measured in layer **2**.

For the case of feldspar, the diffraction pattern recorded on layer **2**
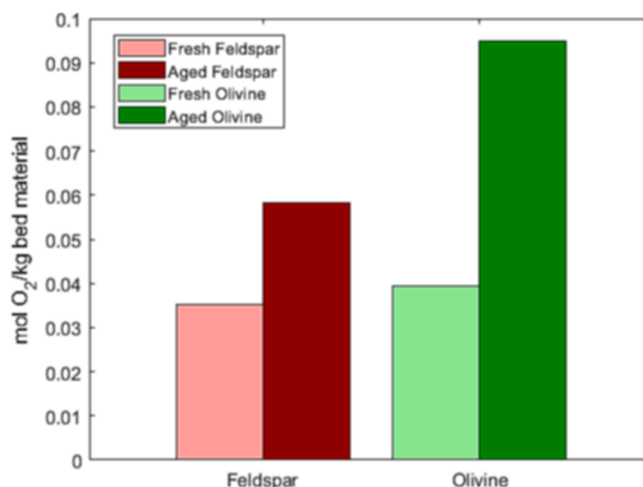

Fig. 14. Oxygen-carrying ability of the materials measured from the difference in O_2 entering and leaving the reactor during the oxidizing step. The materials were investigated as obtained ("fresh") and after 3 days residence time in the gasifier ("aged").

was matched with both periclase (MgO) and hematite (Fe_2O_3). Hematite is a known catalyst for the water–gas shift reaction [42] and was also found previously on used olivine. [44] Periclase is also commonly found with XRD on used olivine, [14,18,21] but it was not found on feldspar. Its presence on the surface of feldspar suggests that the Mg originates from the biomass ash and not from the bed material itself. The diffraction pattern recorded on the location of layer **3** (which contains high concentrations of Si and P) revealed the presence of an amorphous phase. This could influence the capacity of the layer to retain small ash particles, as an amorphous phase is likely to be sticky. The presence of a sticky phase on convex layers could have aided deposition of ash-derived particles and therefore amplified the layer formation on these locations.

3.5. Oxygen-carrying ability

The oxygen-carrying (OC) ability of the materials in their fresh and active state was measured in the batch reactor and the results are shown in Fig. 14. The materials are considered active after 3 days of residence time in the system, as the tar concentration was significantly decreased at that stage [7–8,31]. Comparing the two materials in their fresh state reveals that olivine exhibits an inherent OC ability which is higher than fresh feldspar. This is expected due to the Fe-content in olivine which is able to change its oxidation state from Fe^{3+} at high oxygen partial pressure to Fe^{2+} at lower oxygen partial pressure and thereby transport oxygen. However, in its active state, feldspar exhibits more than twice as much OC as fresh olivine, which can be attributed to the transition metals (i.e., Fe and Mn) found on the surface of aged feldspar. The results of the OC ability of the two materials agrees with the previously discussed Fe- and Mn-rich layer (layer **2**). The oxygen-carrying ability of aged olivine is higher than for aged feldspar. The migration of Fe from the core of the olivine is a possible explanation for the significantly higher OC ability of olivine to feldspar due to the driving force for Fe to diffuse to the surface. While the impact of S cannot be disregarded regarding the oxygen-carrying effect, feldspar exhibits a significant OC ability although no S was found on the surface. This supports the suggested role of transition metals (Fe and Mn).

3.6. Mechanism

The general mechanism for layer formation on feldspar and olivine is summarized in Fig. 15. Ash is deposited onto the bed particles which occurs preferentially on convex areas. A segregation of ash elements
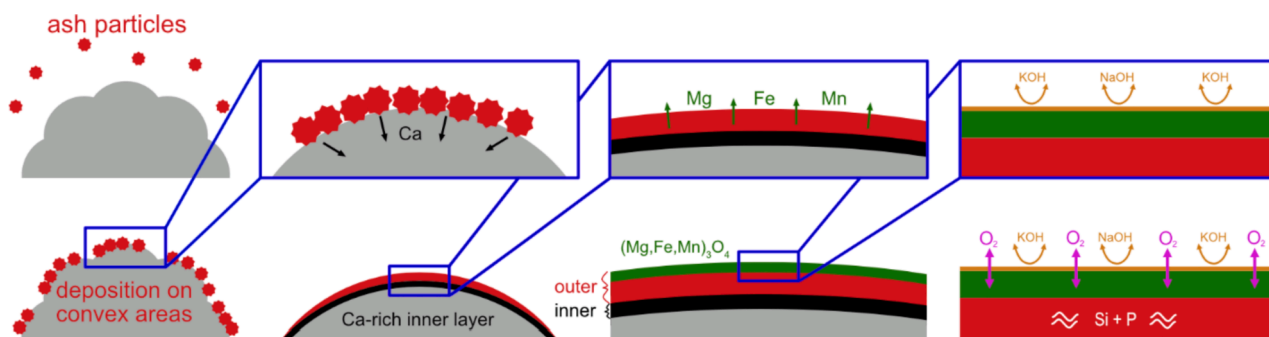
Fig. 15. Schematic depiction of the general mechanism of layer formation found for both olivine and feldspar.

happens, which is influenced by their chemical affinity:

Ash particles preferentially deposit on convex areas of the bed particles.

The Ca from the ash can interact with the bed material which leads to the formation of the homogeneous inner layer.

Oxygen-carrying species such as Fe and Mn are prone to migrate to higher oxygen partial pressures, i.e., the surface of the particles. Mg can form a solid solution with Fe and Mn which is why the three elements (Fe, Mn, Mg) coincide on the surface.

Alkali which can be present as gaseous hydroxides can condensate on the surface of the bed material where they most likely influence the catalytic activity of the particles.

The remaining ash elements (Si and P) are possibly present as a sticky melt which can facilitate deposition of additional ash onto the ash layers.

4. Conclusion

Two different materials (olivine and feldspar) were investigated regarding ash layer formation and the importance of particle morphology was emphasized. The following conclusions were drawn:

Thicker ash layers were formed on convex areas, which impacts especially the inhomogeneous outer layer which is formed due to deposition of ash particles.

The deposition of K_2SO_4 which formed due to the addition of ammonium sulphate appeared preferentially on convex areas.

The inner Ca-rich layer has a constant thickness on convex and concave areas and is therefore likely formed due to the interaction of the deposited outer layer with the bed material particle.

Both materials exhibit a surface layer containing alkali and alkaline earth metal elements which is in line with the observation of their catalytic activity towards limiting tar formation.

A layer containing transition metal elements (Fe and Mn) was found which most likely contributes to the oxygen-carrying ability of both bed materials.

The accumulation of Fe and Mn on the surface and the associated development of an oxygen-carrying effect suggests that for longer exposure times, fuels containing low amounts of Fe and Mn should be utilized.

The influence of the particle morphology on the tendency to form ash layers could aid the selection of starting material. If the formation of a layer is beneficial for the process because the catalytic activity is required to decrease the tar concentration, particles exhibiting convex surface should be utilized. This is likely to be the case for bed material acquired from a sand deposit which usually exhibit a more spherical morphology. Conversely, if the layer formation is detrimental because the development of the oxygen-carrying ability should be avoided, the more rugged features of particles which were acquired from crushed rocks could be used to delay the layer formation.

CRediT authorship contribution statement

Robin Faust: Conceptualization, Methodology, Investigation, Writing – original draft, Visualization. **Ali Valizadeh:** Methodology, Investigation, Writing – original draft. **Ren Qiu:** Methodology, Investigation. **Alyona Tormachen:** Investigation. **Jelena Maric:** Resources, Writing – review & editing. **Teresa Berdugo Vilches:** Resources, Writing – review & editing. **Nils Skoglund:** Methodology, Writing – review & editing. **Martin Seemann:** Resources, Writing – review & editing. **Mats Halvarsson:** Writing – review & editing. **Marcus Öhman:** Methodology, Writing – review & editing. **Pavleta Knutsson:** Conceptualization, Writing – review & editing, Funding acquisition.

Declaration of Competing Interest

The authors declare that they have no known competing financial interests or personal relationships that could have appeared to influence the work reported in this paper.

Data availability

Data will be made available on request.

Appendix A. Supplementary data

Supplementary data to this article can be found online at https://doi.org/10.1016/j.fuel.2022.126387.

References

[1] Larsson A, Seemann M, Neves D, Thunman H. Evaluation of performance of industrial-scale dual fluidized bed gasifiers using the chalmers 2–4-MW$_{th}$ gasifier. Energy Fuels 2013;27:6665–80.
[2] Devi L, et al. Catalytic decomposition of biomass tars: use of dolomite and untreated olivine. Renewable Energy 2005;30:565–87.
[3] Ferreira de Almeida V, Gómez-Barea A, Nilsson S, Tuomi S. Distribution of inorganics and trace elements during waste gasification in a bench-scale fluidized bed. Energy Fuels 2021;35:15802–16.
[4] Rapagna S, Jand N, Kiennemann A, Foscolo PU. Steam-gasification of biomass in a fluidised-bed of olivine particles. Biomass Bioenergy 2000;11.
[5] Knutsson P, et al. Potassium speciation and distribution for the K2CO3 additive-induced activation/deactivation of olivine during gasification of woody biomass. Appl Energy 2019;248:538–44.
[6] Knutsson P, Cantatore V, Seemann M, Tam PL, Panas I. Role of potassium in the enhancement of the catalytic activity of calcium oxide towards tar reduction. Appl Catal B 2018;229:88–95.
[7] Berdugo Vilches T, Marinkovic J, Seemann M, Thunman H. Comparing active bed materials in a dual fluidized bed biomass gasifier: olivine, bauxite, quartz-sand, and ilmenite. Energy Fuels 2016;30:4848–57.

[8] Berguerand N, Berdugo Vilches T. Alkali-feldspar as a catalyst for biomass gasification in a 2-MW indirect gasifier. Energy Fuels 2017;31:1583–92.

[9] Fürsatz K, et al. Impact of residual fuel ash layers on the catalytic activation of K-feldspar regarding the water–gas shift reaction. Biomass Conv Bioref 2021;11: 3–14.

[10] Khan MM, Xu S, Wang C. Catalytic biomass gasification in decoupled dual loop gasification system over alkali-feldspar for hydrogen rich-gas production. Biomass Bioenergy 2022;161:106472.

[11] Trubetskaya A. Reactivity effects of inorganic content in biomass gasification: a review. Energies 2022;15:3137.

[12] Kuba M, Skoglund N, Öhman M, Hofbauer H. A review on bed material particle layer formation and its positive influence on the performance of thermo-chemical biomass conversion in fluidized beds. Fuel 2021;291:120214.

[13] Berdugo Vilches T, et al. Bed material as a catalyst for char gasification: The case of ash-coated olivine activated by K and S addition. Fuel 2018;224:85–93.

[14] Kuba M, et al. Deposit build-up and ash behavior in dual fluid bed steam gasification of logging residues in an industrial power plant. Fuel Process Technol 2015;139:33–41.

[15] Siriwongrungson V, et al. Influence of bed materials on the performance of the Nong Bua dual fluidized bed gasification power plant in Thailand. Biomass Conv Bioref 2020. https://doi.org/10.1007/s13399-020-00908-6.

[16] Morris JD, Daood SS, Chilton S, Nimmo W. Mechanisms and mitigation of agglomeration during fluidized bed combustion of biomass: A review. Fuel 2018; 230:452–73.

[17] Kuba M, et al. Mechanism of layer formation on olivine bed particles in industrial-scale dual fluid bed gasification of wood. Energy Fuels 2016;30:7410–8.

[18] Faust R, Berdugo Vilches T, Malmberg P, Seemann M, Knutsson P. Comparison of ash layer formation mechanisms on si-containing bed material during dual fluidized bed gasification of woody biomass. Energy Fuels 2020;34:8340–52.

[19] Faust R, et al. Layer formation on feldspar bed particles during indirect gasification of wood. 1. K-Feldspar. Energy Fuels 2019;33:7321–32.

[20] Hannl TK, et al. Layer formation on feldspar bed particles during indirect gasification of wood. 2. Na-Feldspar. Energy Fuels 2019;33:7333–46.

[21] Faust R, Sattari M, Maric J, Seemann M, Knutsson P. Microscopic investigation of layer growth during olivine bed material aging during indirect gasification of biomass. Fuel 2020;266:117076.

[22] Pissot S, et al. Development of oxygen transport properties by olivine and feldspar in industrial-scale dual fluidized bed gasification of woody biomass. Energy Fuels 2021;35:9424–36.

[23] He H, Skoglund N, Öhman M. Time-dependent crack layer formation in quartz bed particles during fluidized bed combustion of woody biomass. Energy Fuels 2017; 31:1672–7.

[24] Zhu Z, et al. The role of surface roughness in the wettability and floatability of quartz particles. Appl Surf Sci 2020;527:146799.

[25] Wang M, Wen B, Fan B, Zhang H. Study on adsorption mechanism of silicate adsorbents with different morphologies and pore structures towards formaldehyde in water. Colloids Surf, A 2020;599:124887.

[26] Prouzet E, Boissière C, Kim SS, Pinnavaia TJ. Roughness of mesoporous silica surfaces deduced from adsorption measurements. Microporous Mesoporous Mater 2009;119:9–17.

[27] Wang X, Zhang Q. Role of surface roughness in the wettability, surface energy and flotation kinetics of calcite. Powder Technol 2020;371:55–63.

[28] Darbha GK, Schäfer T, Heberling F, Lüttge A, Fischer C. Retention of latex colloids on calcite as a function of surface roughness and topography. Langmuir 2010;26: 4743–52.

[29] Wang X, Zhang Q. Insight into the influence of surface roughness on the wettability of apatite and dolomite. Minerals 2020;10:114.

[30] Leion H, Frick V, Hildor F. Experimental method and setup for laboratory fluidized bed reactor testing. Energies 2018;11:2505.

[31] Berguerand N, Berdugo Vilches T, Thunman H. Use of alkali-feldspar as bed material for upgrading a biomass-derived producer gas from a gasifier. Chem Eng J 2016;295:80–91.

[32] Kirnbauer F, Hofbauer H. The mechanism of bed material coating in dual fluidized bed biomass steam gasification plants and its impact on plant optimization. Powder Technol 2013;245:94–104.

[33] Wagner K, et al. Layer formation mechanism of K-feldspar in bubbling fluidized bed combustion of phosphorus-lean and phosphorus-rich residual biomass. Appl Energy 2019;248:545–54.

[34] Kirnbauer F, Hofbauer H. Investigations on bed material changes in a dual fluidized bed steam gasification plant in Güssing, Austria. *Energy Fuels* 2011;25:3793–8.

[35] Faust R, et al. Interactions between automotive shredder residue and olivine bed material during indirect fluidized bed gasification. Energy Fuels 2021;35: 15935–49.

[36] Grimm A, Skoglund N, Boström D, Öhman M. Bed agglomeration characteristics in fluidized quartz bed combustion of phosphorus-rich biomass fuels. Energy Fuels 2011;25:937–47.

[37] Brus E, Öhman M, Nordin A. Mechanisms of bed agglomeration during fluidized-bed combustion of biomass fuels. Energy Fuels 2005;19:825–32.

[38] De Geyter S, Öhman M, Boström D, Eriksson M, Nordin A. Effects of non-quartz minerals in natural bed sand on agglomeration characteristics during fluidized bed combustion of biomass fuels. Energy Fuels 2007;21:2663–8.

[39] Kuba M, et al. Thermal stability of bed particle layers on naturally occurring minerals from dual fluid bed gasification of woody biomass. Energy Fuels 2016;30: 8277–85.

[40] Fürsatz K, Fuchs J, Benedikt F, Kuba M, Hofbauer H. Effect of biomass fuel ash and bed material on the product gas composition in DFB steam gasification. Energy 2021;219:119650.

[41] Anis S, Zainal ZA. Tar reduction in biomass producer gas via mechanical, catalytic and thermal methods: A review. Renew Sustain Energy Rev 2011;15:2355–77.

[42] Xie YR, Shen LH, Xiao J, Xie DX, Zhu J. Influences of additives on steam gasification of biomass. 1. Pyrolysis procedure. Energy Fuels 2009;23:5199–205.

[43] Lee D, et al. Recent progress in the catalytic thermochemical conversion process of biomass for biofuels. Chem Eng J 2022;447:137501.

[44] Kuba M, et al. Surface characterization of ash-layered olivine from fluidized bed biomass gasification. Biomass Conv Bioref 2021;11:29–38.

[45] Niu X, Shen L. Ca- and Mg-rich waste as high active carrier for chemical looping gasification of biomass. Chin J Chem Eng 2020. https://doi.org/10.1016/j.cjche.2020.09.024. S1004954120305280.

[46] Hu Q, Wang C-H. Insight into the Fe2O3/CaO-based chemical looping process for biomass conversion. Bioresour Technol 2020;310:123384.